Aerosol Science and Technology

ISSN: (Print) (Online) Journal homepage: https://www.tandfonline.com/loi/uast20

Experimental study on the rebound characteristics of oblique collision of ash particles and the influence of ammonium bisulfate

Shihao Hu, Qi Yin, Yize Zhang, Kefa Cen & Hao Zhou

To cite this article: Shihao Hu, Qi Yin, Yize Zhang, Kefa Cen & Hao Zhou (2022) Experimental study on the rebound characteristics of oblique collision of ash particles and the influence of ammonium bisulfate, Aerosol Science and Technology, 56:11, 1058-1069, DOI: 10.1080/02786826.2022.2120795

To link to this article: https://doi.org/10.1080/02786826.2022.2120795

AEROSOL SCIENCE AND TECHNOLOGY
2022, VOL. 56, NO. 11, 1058–1069
https://doi.org/10.1080/02786826.2022.2120795

Experimental study on the rebound characteristics of oblique collision of ash particles and the influence of ammonium bisulfate

Shihao Hu, Qi Yin, Yize Zhang, Kefa Cen, and Hao Zhou

State Key Laboratory of Clean Energy Utilization, Institute for Thermal Power Engineering, Zhejiang University, Hangzhou, P.R. China

ABSTRACT

The rebound characteristics of oblique collisions of ash particles in a tail flue environment were investigated experimentally. A high speed camera was used to conduct research on the microscopic scale in a temperature and airflow environment similar to the low-temperature region of boiler. Furthermore, this work focused on the influence of impact velocity, impact angle, gas temperature, and ammonium bisulfate on the restitution coefficient. The results indicated that, as the impact velocity increased from 0.4 to 3 m/s, the normal restitution coefficient increased gradually, the tangential restitution coefficient decreased, and the global restitution coefficient remained unchanged. As the impact angle increased from 15° to 75°, the normal restitution coefficient increased and then tended to be stable. The tangential restitution coefficient decreased, reached its minimum value at 60°, and then rose as the impact angle increased. The global restitution coefficient decreased monotonically with an increase of the impact angle. However, in the temperature range of this experiment (250–400 °C), the effect of temperature on the rebound characteristics was not significant. The critical velocity of the ash particles was 0.103 m/s, and the sliding friction coefficient between the ash particles and the target plane was determined to be 0.182. ABS reduced the rebound velocity and rebound angle of ash particles, and the influence of the ABS coating was greater than that of the ABS blending. The impact of ABS on the rebound characteristics of ash particles was mainly reflected in the reduction of normal rebound velocity rather than tangential rebound velocity.

ARTICLE HISTORY
Received 23 April 2022
Accepted 26 August 2022

EDITOR
Jason Olfert

1. Introduction

Ash deposition on heat exchanging surfaces in the low temperature region of boiler is one of the most serious problems in boiler operation. Severe ash deposition can reduce the heat transfer efficiency of the heat exchange surface, aggravate the corrosion of the tail flue (Kleinhans et al. 2018; Naruse et al. 2005; Akiyama et al. 2011), increase the heat loss of the exhaust flue gas and soot blowing frequency, and even affect the stability of the boiler operation. This can cause safety issues and accidents (Wei et al. 2018; Yu et al. 2017; Zhou, Yang, et al. 2014).

The ash deposition process in the low temperature region of a boiler can be simplified into two stages: particles reach the deposition surface, and particles adhere/rebound (Zhou and Hu 2021). The migration and transport process of ash particles to the heat exchange surface during the formation of ash deposits is mainly divided into three mechanisms: inertial impact, turbulent diffusion, and thermophoretic force. These correspond to coarse particles, small particles, and sub-micron particles, respectively (Tomeczek and Wacławiak 2009; Rushdi, Sharma, and Gupta 2004; Mueller et al. 2005). Except for the condensation of alkali metals, the impact and rebound of ash particles is a significant behavior of ash deposition in the low temperature region of a boiler. Therefore, studying the ash particles' resilience characteristics is of great significance for understanding the deposition process in a boiler.

Previous research on ash deposition on heat exchanging surfaces focuses on macroscopic experiments and CFD simulations. Weber et al. (2021) studied the relationship between ash particle temperatures and deposition rates. The experimental results showed that as the temperature increased, the deposition rate decreased initially and then increased. The maximum deposition rate was at 115 and 1200 °C, and the minimum deposition rate was at 600 °C.

CONTACT Hao Zhou zhouhao@zju.edu.cn State Key Laboratory of Clean Energy Utilization, Institute for Thermal Power Engineering, Zhejiang University, Hangzhou 310027, P.R. China.

Supplemental data for this article can be accessed online at https://doi.org/10.1080/02786826.2022.2120795

Zhou, Zhou, et al. (2014) studied the influence of the probe surface temperature on ash deposits using online monitoring technology. A sticking criterion for ash deposition was developed by Yang et al. (2019) to forecast the rebound characteristics of ash deposition according to the energy conservation. This considered the physical and chemical properties of ash particles, deposition surface properties, and furnace operation conditions. A few researchers have investigated the collision and resilience behavior of ash particles at a microscopic scale. Troiano et al. (2016) used Waradur E wax to simulate ash particles to study the coefficient of restitution of particles impacting at different stages of solid/plastic. The effects of particle viscosity, impact velocity, impact angle, target surface viscosity, material, and structure on the coefficient of restitution were also studied. In the study by Gibson et al. (2013), granular coke particles, polystyrene pellets, and high-density polyethylene were used as experimental materials to explore the relationship between particle resilience behavior and particle shape. Xie et al. (2018) studied the oblique collision of ash particles with the metal target surface under ambient temperature and pressure, focusing on the dynamic friction coefficient and critical friction angle. It should be noted that previous research on the impact and rebound of ash particles used similar particles instead of ash particles or was completed in a cold environment.

The condensation of sulfate has a great influence on the rebound characteristics of ash particles. The catalyst used in selective catalytic reduction (SCR) can oxidize SO_2 in flue gas to SO_3, and the generated SO_3 further reacts with escaped ammonia to generate ammonium bisulfate (ABS). ABS is a viscous compound that can condense on the surface of equipment and ash particles in low temperature areas. The ABS in flue gas can form an aerosol, and part of the ABS aerosol may be absorbed by ash particles, increasing the viscosity and reducing the quality of particles. The deposition of ABS can cause blockages and the corrosion of equipment (2016). To the authors' knowledge, there are a few studies on the blended deposition of ABS and ash particles. Vuthaluru and French (2015) found that the deposition on the air preheater contained a large amount of sulfate, which acted as a binder in the formation of deposits. Chen et al. (2017) concluded in his research that ABS was formed at the entrance of a low-pressure economizer, which could increase the viscosity of ash particles and cause serious fouling. Zhou, Zhang, and Zhang (2018) compared the microstructure of ABS blend deposition and the initial fly ash. The ash particles of deposition were agglomerate and formed a dense microstructure. This was because fine particles agglomerate with ABS to form the liquid-bridge, increasing the strength and thermal resistance of deposition. However, previous studies on ABS deposition were carried out at the macroscopic dimension, and the influence of ABS on ash deposition has never been reported at the microscale. In addition, the effects of ABS adhesion on the ash surface and condensation on the impact target surface are different, and have never been studied separately.

The objective of this article was to explore the resilience characteristics of the oblique collision of ash particles in a tail flue environment. A high speed camera was used to conduct experimental research in a temperature and airflow environment similar to the low temperature region of a boiler. This study focuses on the influence of impact velocity, impact angle, and gas temperature on the restitution coefficient. The critical velocity and dynamic friction coefficient of the particles were also given. In addition, the effect of ABS on the impact characteristics of ash particles was also reported.

2. Theoretical background

The process of ash particles depositing on the heat exchange surface can be simplified to the rebound process of the ash particles colliding with the target surface. When the particle is in contact with the impact plane, the forces on the particle include friction, thermophoresis, and surface forces. The surface forces are caused by adhesion and the van der Waals force (Abd-Elhady and Malayeri 2013). In collision dynamics, the restitution coefficient is a common parameter that reflects the energy consumption during impact. The definition of restitution coefficient e is the percentage of rebound velocity to incident velocity (Zhou et al. 2016):

$$e_g = \left|\frac{V_r}{V_i}\right| = \sqrt{1 - \frac{E_d}{E}}, \tag{1}$$

where V_i and V_r are the impact and rebound velocities of ash particles, respectively, E is the kinetic energy of the incident particles (angular momentum is ignored), and E_d is the energy dissipation during impact. According to Liu, Li, and Yao (2011), energy dissipation can be divided into two parts, first-contact energy loss and energy dissipation through damping effects (friction and adhesion) or plastic deformation. The first-contact energy loss is independent of the impact velocity. The energy loss caused by plastic

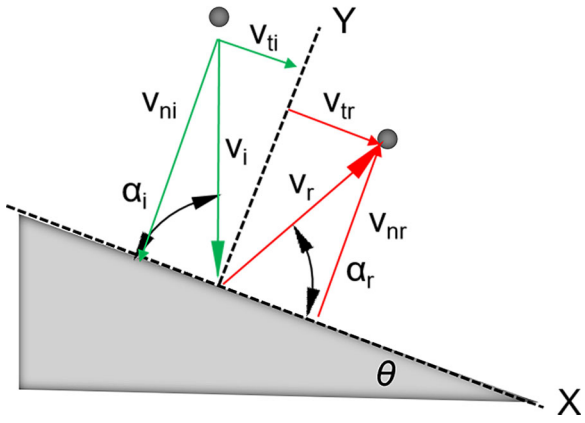

Figure 1. The schematic diagram of the particle oblique collision.

deformation and damping effects is closely related to the impact velocity. When the collision is a perfect elastic collision, the coefficient of restitution is 1. When the ash particle dissipates all the kinetic energy and attaches to the target surface, the coefficient of restitution is 0.

For oblique collisions, the velocity of the particles consists of a normal velocity perpendicular to the impact target and a tangential velocity parallel to the target plan. Therefore, the coefficient of restitution can also be separated into the normal and tangential coefficients of restitution. The schematic diagram of oblique collision is shown in Figure 1. The normal and tangential restitution coefficients are defined as follows (Troiano et al. 2016, 2017):

$$e_n = \left|\frac{V_{nr}}{V_{ni}}\right|, \tag{2}$$

$$e_t = \left|\frac{V_{tr}}{V_{ti}}\right|, \tag{3}$$

where V_{ni} and V_{nr} are the normal components of the incidence and rebound velocity, respectively. V_{ti} and V_{tr} are the tangential components of the incidence and rebound velocity, respectively.

According to rigid body theory, for an oblique impact, particles with a small impact angle will slide on the target surface. At this time, the coefficients of restitution and the impact angle have the following relationship, in the regime of sliding (Troiano et al. 2016; Xie et al. 2018):

$$e_t = -f(1 + e_n)\tan\alpha_i + 1, \tag{4}$$

where f represents the ratio of the tangential component to the normal component of the impulse. When the inclination angle of the target is too large, that is, the impact angle is below the critical value, gross slipping is expected to occur, and the sliding friction coefficient μ_f is equal to f (Xie et al. 2018).

3. Experimental

3.1. Experimental apparatus and materials

The experimental system of the ash particle impact is shown in Figure 2. The system consists of a vertical electric heating furnace, a quartz tube (inner diameter 30 mm, length 1300 mm), a dropper, one air compressor (outstanding 800 W-30L), an inclined target plane (304 stainless steel), a high speed camera (AOS S-PRI plus high speed camera), and a laser transmitter (MGL-N-532-4W14010076). A batch of particles was placed in the dropper before the experiment (to preheat to the required temperature) and then released during the experiment. The transported air entered the quartz tube from the upper side, and the flow was controlled by a mass flowmeter (Alicate 21-1-00-1-250-200-KM6003). The impact velocity of the ash particles was controlled by the airflow and settling velocity of the particles. The measurement and calculation methods of the impact velocity were shown in Equation (S1). During the experiment, the ash particles were released from the dropper. They then passed through the furnace next to the hot air, and impacted the target (not heated) plane 5 cm below the quartz tube.

A digital high speed camera was arranged at the same level as the target plane. The camera was equipped with a five times magnification zoom lens and a telephoto lens. The camera used a CMOS APS sensor that was connected to the computer through a cat 5e Ethernet cable for displaying, recording, and saving experimental images. Since the exposure time required for the experiment was extremely short, a laser was used as the light source. The detailed parameters of the experimental system are shown in the Supplementary Material.

The ash particles used in the experiment were all sampled from the bag filter of an industrial power plant. The composition of ash was measured by X-ray fluorescence (XRF), as shown in Table 1. The ash particles are mainly composed of Al_2O_3, SiO_2, CaO, Fe_2O_3, while the content of alkali metals is relatively small. The ash particles used in the experiment have a particle size of 21–58 μm, the particle size distribution of the particles is shown in Figure S1. The target surface material is stainless steel (roughness is 0.2 μm).

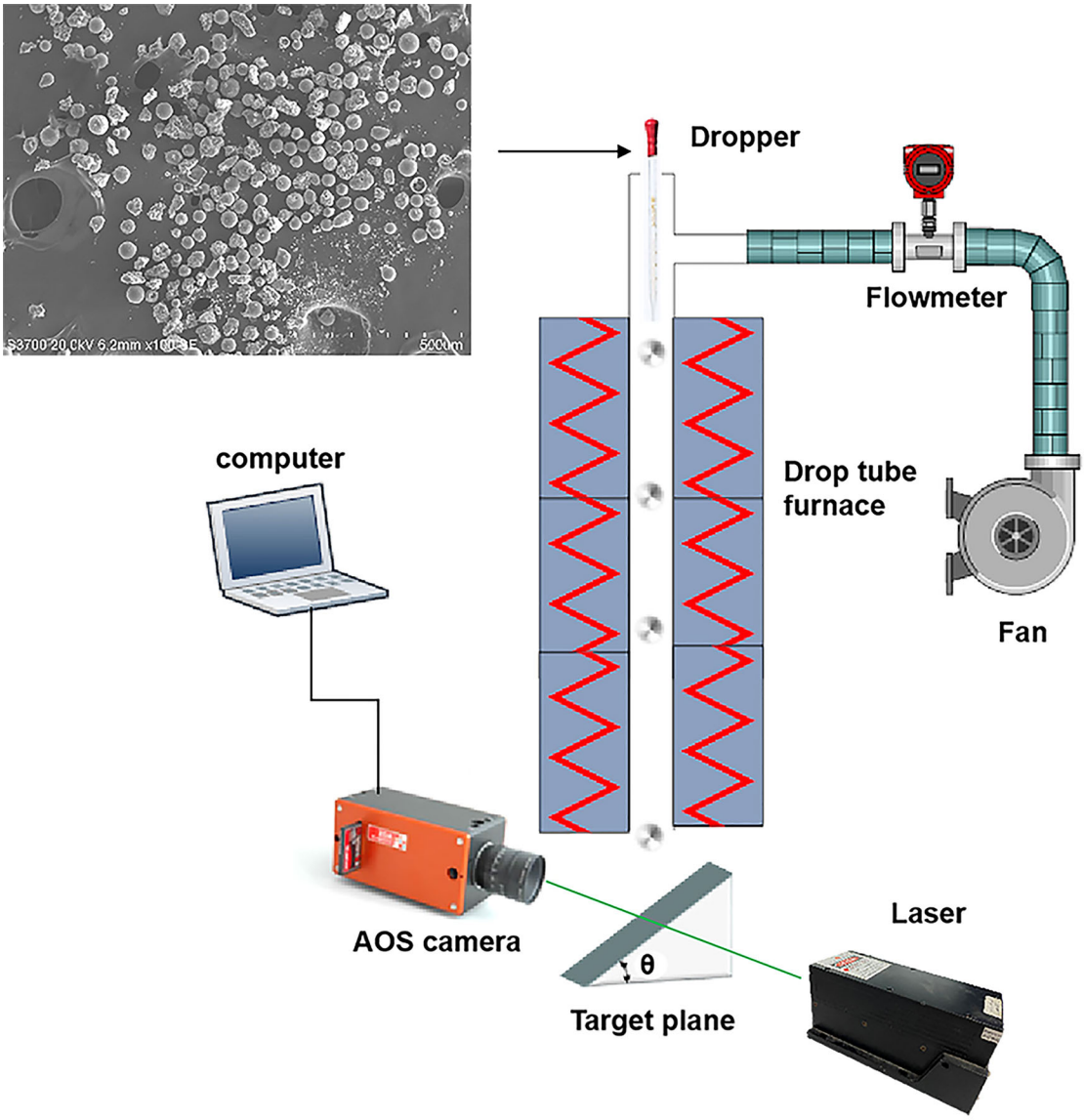

Figure 2. The experimental system of the ash particle impact.

Table 1. Ash compositions.

Item	Al_2O_3	CaO	Fe_2O_3	K_2O	MgO	Na_2O	SiO_2	SO_3	TiO_2	P_2O_5
wt%	27.80	14.66	13.18	1.79	1.43	0.76	36.24	1.34	1.81	0.30

3.2. Operating conditions

To study the impact of incident velocity, incident angle, and gas temperature on the rebound characteristics of oblique collisions of ash particles, we used the experimental conditions 1–3 shown in Table 2. According to the method of controlling variables, the impact speed, impact angle, and gas temperature were changed successively while the other two parameters were fixed. The design of conditions 4 and 5 used two methods to study the effects of ABS on particle impact in the low temperature region of the boiler. In condition 4 (ABS coating), the surface of the impact target was coated with a layer of ABS. A certain concentration of ABS solution was sprayed into the flue at a uniform speed, and the flue gas temperature was set to 350 °C. A cold impact plate was placed at the end of the flue, and the ABS in the flue gas condensed evenly on the impact surface. The thickness of ABS layer was about $30 \pm 2\,\mu$m, and the roughness was $20\,\mu$m. In condition 5 (ABS blending), the ash particles and ABS were uniformly mixed at a mass ratio of 30:1, then the mixture was melted at 180 °C for 2 h. The ash particles were used for impact experiments after cooling. To ensure the accuracy of the experiment, each case was repeated three times, at least 50 particles were selected for one parameter condition, and then the impact results of each particle were averaged.

Table 2. Experimental parameter.

Condition	1 Original/impact velocity	2 Impact angle	3 Furnace temperature	4 ABS coating	5 ABS blending
Impact velocity (m/s)	0.4–3.0	1.5	1.0	0.5–2.0	0.5–2.0
Impact angle (°)	60	15, 30, 45, 60, 75	60	60	60
Furnace temperature (°C)	300	300	250, 300, 350, 400	300	300
Particle	Ash				Ash + ABS
Particle diameter (μm)	21–58				
Target material	Stainless steel			Stainless steel + ABS	Stainless steel

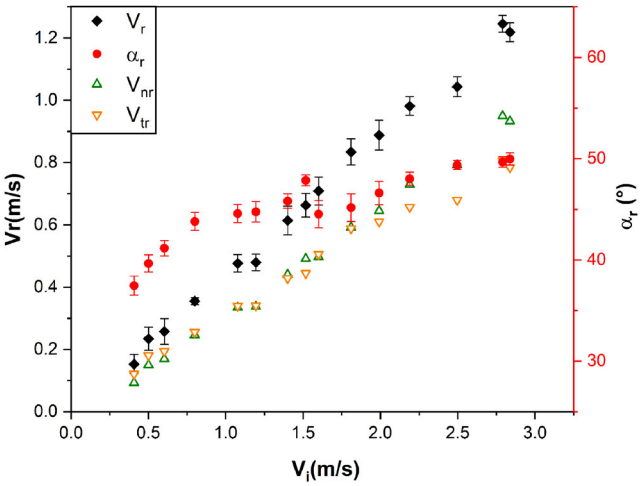

Figure 3. The dependence of the rebound velocity and angle on the impact velocity. $T = 300\,^{\circ}C$, $\alpha_i = 60^{\circ}$.

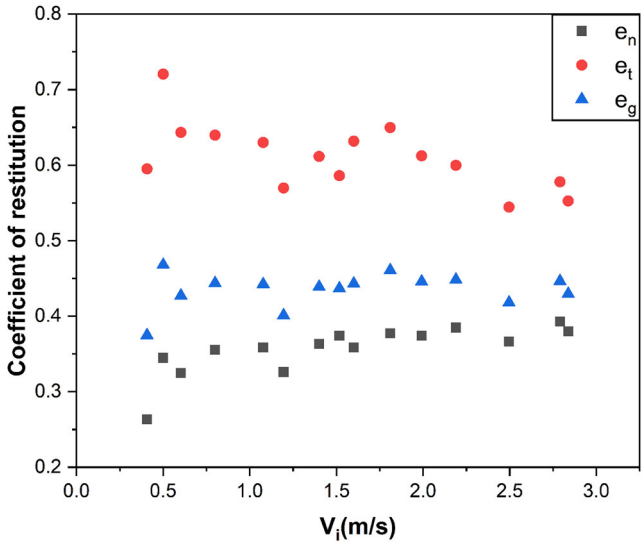

Figure 4. The dependence of the coefficient of restitution on the impact velocity. $T = 300\,^{\circ}C$, $\alpha_i = 60^{\circ}$.

4. Result and discussion

4.1. The effect of impact velocity on rebound characteristics

Figure 3 reports the variation of rebound velocity and angle as the impact velocity increases from 0.4 to 2.8 m/s. When the gas temperature and impact angle are determined, the rebound velocity and angle increase with increasing impact velocity in the investigated range, from 0.15 m/s, 37.4° (impact velocity 0.4 m/s) to 1.21 m/s, 49.9° (impact velocity 2.8 m/s), respectively. The rebound velocity is always less than the impact velocity, and similarly, the rebound angle is also smaller than the impact angle. When the impact angle is 60°, the tangential rebound velocity is close to the normal rebound velocity, and they both increase with the increase of impact velocity. When the impact velocity is small, the tangential rebound velocity is greater than the normal rebound velocity. However, as the impact velocity increases above 1.5 m/s, this relative relationship is reversed. According to Equations (1)–(3), the coefficients of restitution (e.g., e_n, e_t) of ash particles at different impact velocities are calculated, as shown in Figure 4. The tangential restitution coefficient is larger than the normal restitution coefficient at all experimental velocities. The global restitution coefficient is maintained at about 0.44, which is independent of the impact velocity. Correspondingly, in Figure 3, the rebound velocity increases linearly with the impact velocity. No matter how the impact velocity changes, the proportion of energy consumed by the impact remains constant. The normal coefficient of restitution increases, while the tangential restitution coefficient decreases gradually with a rise in impact velocity. According to research of Wall et al. (1990), in the low velocity impact range the energy loss is a function of the target material due to the adhesion surface energy which depends on the surface composition. When the impact velocity is slightly greater than the critical velocity, the curve of e_n–V_{ni} has a quite steep slope, but the slope gradually decreases with the increase of the impact velocity until the plastic yield velocity. This phenomenon can be attributed to the change of the ratio of attractive and repulsive force with collision intensity. The ash particles are subjected to a variety of fluid forces in the flow field, including drag, buoyancy, lift, and thermophoretic forces generated by the temperature gradient (Yang et al. 2017). Thoronton and Ning (1998) proposed the relationship between the normal restitution coefficient and normal incident velocity of elastic perfectly plastic, adhesive spheres based on JKR

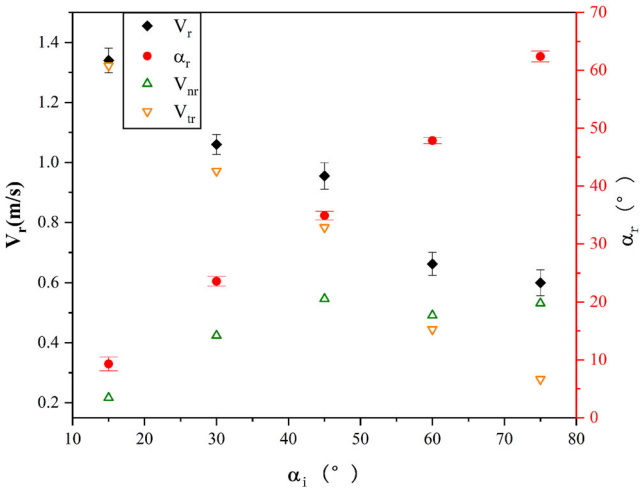

Figure 5. The dependence of the rebound velocity and angle on the impact angle. $T = 300\,^{\circ}\mathrm{C}$, $V_i = 1.5$ m/s.

theory. When $V_i \leq V_s$, the ash particles deform elastically after the collision. At this time, the initial energy of the particles is less than the energy loss, so the particles adhere to the impact surface. The restitution coefficient is 0. When the normal impact velocity exceeds the critical velocity, the normal restitution coefficient increases with impact velocity, but the growth rate decreases until it reaches the peak. Then the normal restitution coefficient begins to decrease, and the rate of decrease increases gradually. The relationship between e_n and V_{ni} is expressed as follows:

$$e_n{}^2 = \begin{cases} 0, & V_{ni} \leq V_s, \\ 1 - \dfrac{V_s^2}{V_{ni}^2}, & V_s \leq V_{ni} \leq V_y, \\ \dfrac{6\sqrt{3}}{5}\left[1 - \dfrac{1}{6}\left(\dfrac{V_y}{V_{ni}}\right)^2\right] \times \left[\dfrac{\left(\frac{V_y}{V_{ni}}\right)}{\left(\frac{V_y}{V_{ni}}\right) + 2\sqrt{\frac{6}{5} - \frac{1}{5}\left(\frac{V_y}{V_{ni}}\right)^2}}\right]^{\frac{1}{2}} - \dfrac{V_s^2}{V_{ni}^2}, & V_y < V_{ni}, \end{cases} \tag{5}$$

where V_s represents the critical velocity of the particles and V_y represents the plastic yield velocity of the particles.

In Figure 4, the increase of the normal restitution coefficient indicates that the normal impact velocity of the experiment is still in the $V_s \leq V_{ni} \leq V_y$ range. When the impact velocity of the particles remains the same, the coefficient of restitution is negatively correlated with the critical velocity. The critical velocity is related to the properties of the particles and target surface material. The form of equation $e_n{}^2 = 1 - \frac{V_s^2}{V_{ni}^2}$ is transformed into $1 - e_n{}^2 = V_s^2 \frac{1}{V_{ni}^2}$. Figure S3 in the Supplementary Material shows values of $1 - e_n{}^2$ plotted against $\frac{1}{V_{ni}^2}$, and the gradient of the fitted curve is V_s^2. Therefore, the critical velocity of the experimental ash particles is calculated as 0.103 m/s.

4.2. The effect of impact angle on rebound characteristics

Figure 5 reports relationship between rebound velocity and angle with impact angle. There is a negative correlation between rebound speed and impact angle, that is, a decrease of impact angle will lead to an increase in rebound speed. When the impact occurs with an impact angle of 15°, the rebound velocity reaches a maximum of 1.34 m/s, and the minimum value of 0.60 m/s occurs when the impact angle is 75°. On the contrary, the rebound angle increases from 9.3° to 62.4°, while the impact angle changes from 15° to 75°. The impact angle is slightly larger than the rebound angle, and the change of impact angle causes a monotonous alter in the rebound angle. The tangential rebound velocity decreases with the increase of the impact angle, while the normal rebound velocity increases first and then maintains a stable value.

Figure 6 reports the corresponding relationship between the restitution coefficient and impact angle. It can be concluded from Figure 6 that the tangential restitution coefficient is always greater than the normal restitution coefficient, and all restitution coefficients are less than 1. As the impact angle rises, the normal restitution coefficient decreases, then tends to stability, which is consistent with the conclusion by Sommerfeld. In the study of the particle-wall collision process, Sommerfeld and Huber (1999) concluded that the curve of the normal restitution coefficient shows a decrease from 1 at $\alpha_i = 0$ to an asymptotic value. With further increasing impact angle the restitution coefficient is almost constant. The asymptotic

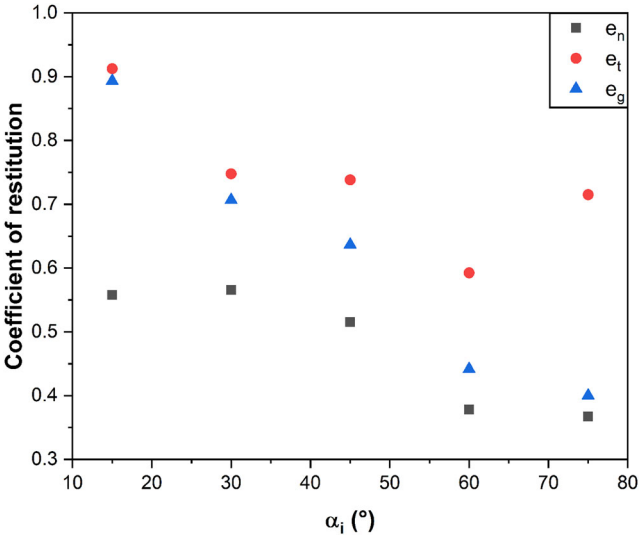

Figure 6. The dependence of the coefficient of restitution on the impact angle. $T = 300\,^{\circ}C$, $V_i = 1.5$ m/s.

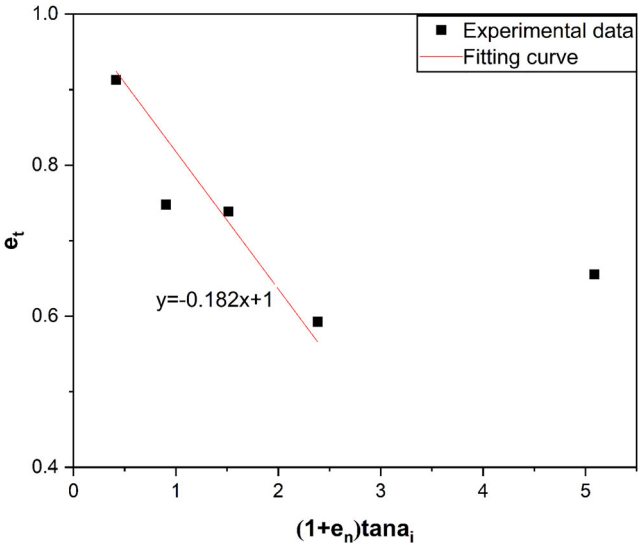

Figure 7. The dependence of e_t on $(1 + e_n)\tan\alpha_i$

values are clearly correlated with the wall material. This may be caused by the ash particles not being perfectly spherical and the impact surface not being completely smooth. The maximum value of the normal restitution coefficient is about 0.57. When the impact angle increases to 60°, the final stable normal restitution coefficient is approximately 0.37. The tangential coefficient of restitution initially decreases, reaching a minimum value of 0.59 at 60°, and then rises with an increasing impact angle. According to Gorham and Kharaz (2000), oblique collision can be divided into three regions by the impact angle, the gross sliding region, micro sliding region and sticking region. The maximum and minimum values of the tangential restitution coefficient appear in the micro slip region and gross slip region, respectively. The minimum value of 0.59 of the tangential restitution coefficient appears when the impact angle is 60°. When the impact angle is 15°, the tangential restitution coefficient reaches its maximum value of 0.91 (close to 1). A smaller impact angle indicates a higher global restitution coefficient, which means the proportion of energy loss caused by collision increases as the angle of impact increases. When collision occurs at a small impact angle, the global restitution coefficient is approximately equal to the tangential restitution coefficient. At a large impact angle, the global restitution coefficient is approximately equal to the normal restitution coefficient. The global restitution coefficient can be expressed by the distributed coefficient of restitution:

$$e_g = \left|\frac{V_r}{V_i}\right| = \sqrt{\frac{{V_{tr}}^2 + {V_{nr}}^2}{{V_i}^2}} = \sqrt{\frac{{V_{tr}}^2}{\frac{{V_{ti}}^2}{\cos^2\alpha_i}} + \frac{{V_{nr}}^2}{\frac{{V_{ni}}^2}{\sin^2\alpha_i}}}$$
$$= \sqrt{{e_t}^2\cos^2\alpha_i + {e_n}^2\sin^2\alpha_i}. \quad (10)$$

According to Equation (10), when the impact angle α_i approaches 90°, the collision is equivalent to a normal impact and the global restitution coefficient is close to the normal restitution coefficient. When the impact angle α_i approaches 0°, the global restitution coefficient approaches the tangential restitution coefficient.

According to Equation (4), the corresponding relationship diagram between e_t and $(1 + e_n)\tan\alpha_i$ is obtained, as shown in Figure 7. The black dots indicate the experimental results, and the red straight line is the fitted curve. When the impact angle is less than 60°, the experimental data (four points on the left) is in agreement with the fitted curve. However, the experimental data of 75° (rightmost point) deviates greatly from the fitted curve. This is because sliding occurs when the impact angle is less than 60°. The equation of the fitted curve is $y = -0.182x + 1$, so the sliding friction coefficient of the target plane is 0.182.

4.3. The effect of gas temperature on rebound characteristics

Table 3 shows the temperature at different vertical distances from the impact plane under different experimental temperatures. The temperatures at the impact plane are 148, 208, 249, and 289 °C, when the experimental temperature is 250, 300, 350, and 400 °C, respectively. The lowest temperature occurs at 1,250 mm from the impact plane, where the gas enters the quartz tube. The highest temperature occurs at

Table 3. The temperature at different vertical distances from the impact plane.

Vertical distance from impact plane (mm)	Experimental temperature (°C)			
	250	300	350	400
0	148	208	249	289
50	176	231	276	328
350	225	273	310	359
650	248	294	345	398
950	249	311	360	411
1250	95	131	185	233

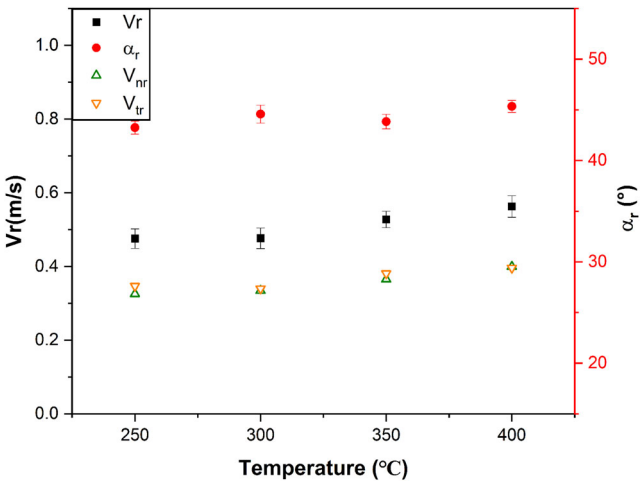

Figure 8. The dependence of the rebound velocity and angle on the experimental temperature.

950 mm from the impact plane, which is the heating part of the furnace. The temperature is about 10 °C higher than the set temperature.

Figure 8 shows the change in rebound velocity and angle of the ash particles with the experimental temperature when the impact angle is 60° and the impact velocity is 1 m/s. According to Figure 8, as the experimental temperature rises from 250 to 400 °C, the rebound velocity and rebound angle increase from 0.47 m/s and 43.2° to 0.56 m/s and 45.3°, respectively. The tangential rebound velocity is similar to the normal rebound velocity and is maintained at around 0.35 m/s. It can be determined that the changes in temperature field and flow field around the impact plane surface have a slight effect on the rebound characteristics of the particles.

Figure 9 shows the trend of restitution coefficient with experimental temperature. With an experimental temperature increase from 250 to 400 °C, all restitution coefficients increase slightly. The normal restitution coefficient increases from 0.37 to 0.46, the tangential restitution coefficient increases from 0.69 to 0.79, and the global restitution coefficient increases from 0.47 to 0.56. In the range of this experimental investigation, the influence of temperature on the

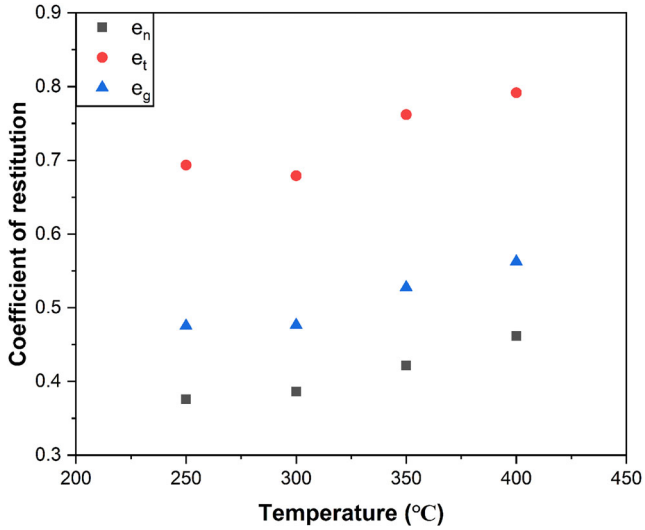

Figure 9. The dependence of the coefficient of restitution on the experimental temperature. $\alpha_i = 60°$, $V_i = 1.0$ m/s.

rebound characteristics of particles is not significant. This can be explained by the fact that the temperature gradient near the target surface is not large, and the size of the ash particles used in the experiment is 21–58 μm. The thermophoretic force has little effect on the experimental particles. There are several studies, such as Cameron and Goerg-Wood (1999) and Walker, Homsy, and Geyling (1979), that indicate the dominant role of thermophoresis for the deposition of particles in a diameter range of 0.1–10 μm. In addition, the melting temperature of ash particles is higher than 1200 °C, so the adhesive force of particles at the gas temperature has no obvious change compared with the force at the atmospheric temperature. It can be speculated that the influence of the gas temperature on the rebound characteristics of the ash particles is mainly caused by the slight differences in the flow field near the target surface, the viscosity of the target surface, and the ash particles.

4.4. The effect of ABS on rebound characteristics

Figure 10 shows the variation curves of the rebound velocity on the impact velocity under conditions 1, 4, and 5. In the three conditions, the rebound velocity of the ash particles increases with an increase in impact velocity. When the impact velocity is constant, the rebound velocity of the original ash particles is the largest, and that of the ABS coating is the smallest. For the original ash particles, the difference between the tangential and normal rebound velocities is small. However, under the influence of ABS, especially in the case of ABS coating, the normal rebound velocity is much smaller than the tangential rebound velocity.

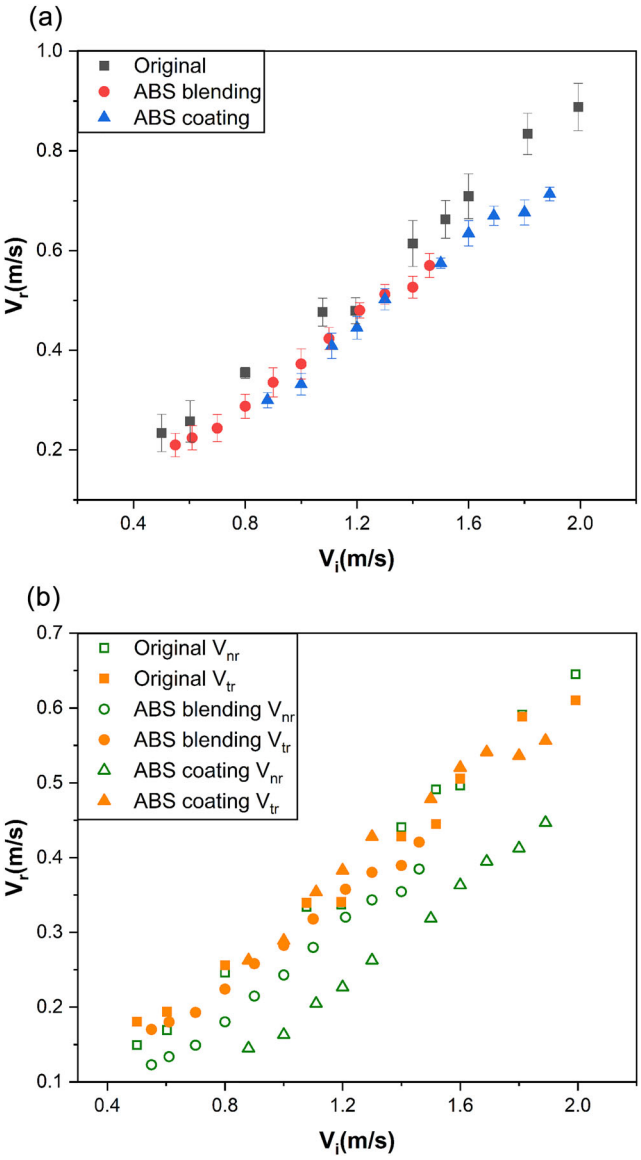

Figure 10. The dependence of the rebound velocity on the impact velocity. Original (condition 1), ABS coating (condition 4), ABS blending (condition 5), $T = 300\,^{\circ}C$, $\alpha_i = 60^{\circ}$.

The results show that ABS has an influence on the impact rebound characteristics of ash particles, and the influence of the ABS coating is greater than that of ABS blending. The temperature of the experiment is 300 °C, while the melting point of ABS is 147 °C and the molten ABS is a sticky substance. When the ash particles mixed with ABS enter the quartz tube, the ABS attached to the surface of the ash particles melts and forms a liquid film. Similarly, the temperature of the impact surface is 208 °C, and the molten ABS liquid film covers the impact surface, which greatly increases the stickiness of the impact surface. When the ash particles reach the impact surface, the adhesion force increases compared with the original ash, resulting in a decrease of rebound velocity.

Figure 11 shows the variation curves of the rebound angle of ash particles on impact velocity under working conditions 1, 4, and 5. The rebound angle increases slightly with an increase in impact velocity. The influence of ABS on the rebound angle of ash particles seems to be much greater than the rebound velocity. At the same impact velocity, the rebound angle of ABS blending is slightly lower than that of the original ash particles, while the decreasing amplitude of ABS coating is more obvious. In order to analyze the reasons behind these results, we observed the ABS blending and original ash particles by scanning electron microscope (SEM) as shown in Figure S4 of the Supplementary Material. Figure S4a shows the image of the original ash particles, most of which have a smooth surface. Figure S4b shows the image of ABS blending ash particles. ABS adhesion can be observed on the surface of the ash particles, but the adhesion is not omni-directional. When the ABS blending ash particles hit the impact target, two situations may occur: the contact surface is the original ash particles, or the contact surface is ABS. Therefore, the influence of ABS blending on the impact characteristics of ash particles is closely related to the blending ratio. Liang (2014) found that ABS content has a large influence on the adhesion of ash particles. Under the same humidity, when the mass ratio of ash to ABS is 150:1, the adhesion is 1.2 times that of original ash. When the ratio increases to 30:1, the adhesion increases to 4.27 times that of the original ash, and the melting of ABS further increases the adhesion of ash particles.

Figure 12 shows the variation curves of the restitution coefficient on the impact velocity under working conditions 1, 4, and 5. Under all working conditions, the normal restitution coefficient increases with an increase in impact velocity. The global restitution coefficient remains almost unchanged and fluctuates within a certain range. The average global restitution coefficients of the three working conditions are 0.44, 0.38, and 0.37, respectively. The maximum value of the tangential restitution coefficient of the original and ABS blending ash particles appears at the minimum impact velocity. As the impact velocity increases, the tangential restitution coefficient gradually decreases and tends to stability. However, the tangential restitution coefficient of ABS coating fluctuates slightly in a small range. Combining with Figure 10, we can find that the effect of ABS on the tangential restitution coefficient is much smaller than that of the normal restitution coefficient. This is due to the liquid film produced by ABS melting. The tangential

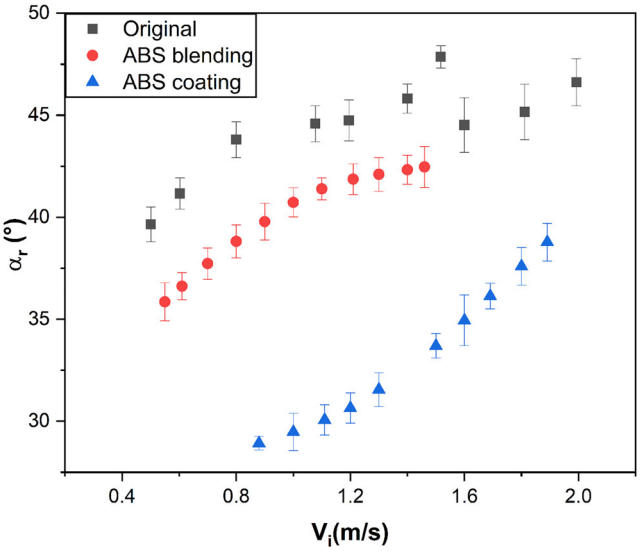

Figure 11. The dependence of the rebound angle on the impact velocity. Original (condition 1), ABS coating (condition 4), ABS blending (condition 5), $T = 300\,^{\circ}C$, $\alpha_i = 60^{\circ}$.

restitution coefficient of the three conditions is almost the same in the impact velocity range of 1.0–1.8 m/s. According to the research of Buck et al. (2017), the liquid film has little effect on the tangential and rotational energy, but greatly reduces the normal energy of particles.

Figure S5 in the Supplementary Material shows the fitting curves of $1 - e_n{}^2$ and $\frac{1}{V_{ni}^2}$ for the ABS blending and ABS coating. The critical velocities of the ABS blending and ABS coating can be calculated from the slopes of the fitting curve, which are 0.141 and 0.229 m/s, respectively.

Combined with Figures 10–12, it can be concluded that the impact of ABS on the rebound characteristics of ash particles is mainly reflected in the reduction in rebound angle rather than rebound velocity. During the experiment, we observed some interesting phenomena. When hitting the impact target coated with ABS, a few ash particles slide on the impact plane for a certain distance and then rebound. It can be speculated that this is also a way for ABS to reduce the rebound energy of impact particles and increase the capture rate.

5. Conclusion

This article studies the oblique collision of ash particles in a tail flue environment. A digital high speed camera is used to study the impact rebound characteristics of ash particles at a microscopic scale. The effects of impact velocity, impact angle, and gas

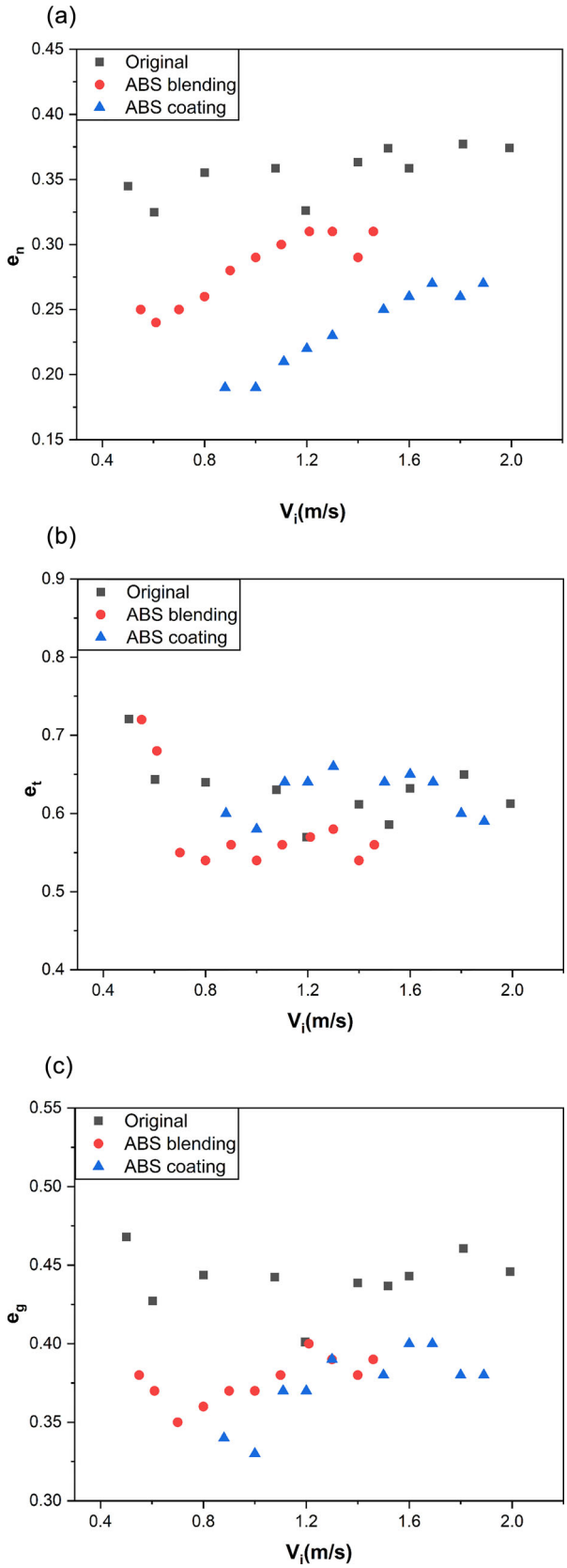

Figure 12. The dependence of the coefficient of restitution on the impact velocity. Original (condition 1), ABS coating (condition 4), ABS blending (condition 5), $T = 300\,^{\circ}C$, $\alpha_i = 60^{\circ}$.

temperature are analyzed. In addition, the effect of ABS on the impact characteristics of ash particles is also reported. The significant results are as follows.

1. The rebound velocity and angle increase as the impact velocity increases in the investigated range. As the impact velocity increases, the normal restitution coefficient increases gradually, and the tangential restitution coefficient decreases. The global restitution coefficient remains unchanged. According to the correlation between e_n and V_{ni}, the critical velocity of the experimental ash particles is calculated to be 0.103 m/s.
2. The increase of impact angle will lead to an increase of rebound angle and a decrease of rebound velocity. As the impact angle rises, the normal restitution coefficient decreases, then tends to stability. The minimum value of the tangential restitution coefficient is 0.59 ($\alpha_i = 60°$) and the maximum value is 0.91 ($\alpha_i = 15°$). The sliding friction coefficient between the ash particle and target plane is determined to be 0.182.
3. The effect of gas temperature on the rebound characteristics of ash particles is not significant. When the gas temperature increases from 250 to 400 °C, the normal restitution coefficient and global restitution coefficient increase slightly. The tangential restitution coefficient is almost unchanged.
4. ABS can reduce the rebound velocity and rebound angle of ash particles, and the influence of ABS coating is greater than that of ABS blending. The critical velocities of ABS blending and ABS coating are 0.141 and 0.229 m/s, respectively. The impact of ABS on the rebound characteristics of ash particles is mainly reflected in the reduction of normal rebound velocity rather than tangential rebound velocity.

Nomenclature

ABS	ammonium bisulfate
CFD	computational fluid dynamics
SCR	selective catalytic reduction
PID	proportional integral derivative
XRF	X-ray fluorescence
AOS	alpha and omega semiconductor
CMOS	complementary metal oxide semiconductor
APS	active pixel sensor
SEM	scanning electron microscope
V_i	the impact velocity of ash particles (m/s)
V_r	the rebound velocity of ash particles (m/s)
α_i	the impact angle of ash particles (°)
α_r	the rebound angle of ash particles (°)
e_g	the global restitution coefficient
e_n	the normal restitution coefficient
e_t	the tangential restitution coefficient
E	the kinetic energy of incident particles
E_d	the energy consumed during the impact
$V_{ni(\mathrm{m/s})}$	the normal components of the incidence velocity
$V_{nr(\mathrm{m/s})}$	the normal components of the rebound velocity
$V_{ti(\mathrm{m/s})}$	the tangential components of the incidence velocity
$V_{tr(\mathrm{m/s})}$	the tangential components of the rebound velocity
μ_f	the sliding friction coefficient
n	the magnification of the camera
θ	the tilt angle of the target plane (°)
$V_{s(\mathrm{m/s})}$	the critical velocity of the particles (the critical velocity is the velocity at which the particle motion stops when it collides with a surface)
$V_{y(\mathrm{m/s})}$	the plastic yield velocity of the particles

Funding

This work was supported by the China National Funds for Distinguished Young Scientists (No. 51825605).

References

Abd-Elhady, M. S., and M. R. Malayeri. 2013. Asymptotic characteristics of particulate deposit formation in exhaust gas recirculation (EGR) coolers. *Appl. Therm. Eng.* 60 (1–2):96–104. doi:10.1016/j.applthermaleng.2013.06.038.

Akiyama, K., H. Pak, Y. Takubo, T. Tada, Y. Ueki, R. Yoshiie, and I. Naruse. 2011. Ash deposition behavior of upgraded brown coal in pulverized coal combustion boiler. *Fuel Process. Technol.* 92 (7):1355–61. doi:10.1016/j.fuproc.2011.02.016.

Buck, B., Y. Tang, S. Heinrich, N. G. Deen, and J. A. M. Kuipers. 2017. Collision dynamics of wet solids: Rebound and rotation. *Powder Technol.* 316:218–24. doi:10.1016/j.powtec.2016.12.088.

Cameron, J., and K. Goerg-Wood. 1999. Role of thermophoresis in the deposition of fume particles resulting from the combustion of high inorganic containing fuels with reference to kraft black liquor. *Fuel Process. Technol.* 60 (1):49–68. doi:10.1016/S0378-3820(99)00025-9.

Chen, H., J. Jiao, P. Pan, Q. Zhao, and Y. Wang. 2017. Deposit formation of the low-pressure economizer in a coal-fired thermal power plant. *Energy Fuels* 31 (5): 4791–98. doi:10.1021/acs.energyfuels.6b03507.

Gibson, L. M., B. Gopalan, S. V. Pisupati, and L. J. Shadle. 2013. Image analysis measurements of particle coefficient of restitution for coal gasification applications. *Powder Technol.* 247:30–43. doi:10.1016/j.powtec.2013.06.001.

Gorham, D., and A. Kharaz. 2000. The measurement of particle rebound characteristics. *Powder Technol.* 112 (3): 193–202. doi:10.1016/S0032-5910(00)00293-X.

Kleinhans, U., C. Wieland, F. J. Frandsen, and H. Spliethoff. 2018. Ash formation and deposition in coal and biomass fired combustion systems: Progress and challenges in the field of ash particle sticking and rebound behavior. *Prog. Energy Combust. Sci.* 68:65–168. doi:10.1016/j.pecs.2018.02.001.

Liang, D. 2014. Experimental research on the effects to flue ash particles characteristics of NH_4HSO_4 generating during the denitrification process. PhD diss., Shandong University (in Chinese).

Liu, G., S. Li, and Q. Yao. 2011. A JKR-based dynamic model for the impact of micro-particle with a flat surface. *Powder Technol.* 207 (1–3):215–23. doi:10.1016/j.powtec.2010.11.002.

Mueller, C., M. Selenius, M. Theis, B. Skrifvars, R. Backman, M. Hupa, and H. Tran. 2005. Deposition behaviour of molten alkali-rich fly ashes—Development of a submodel for CFD applications. *Proc. Combust. Inst.* 30 (2):2991–98. doi:10.1016/j.proci.2004.08.116.

Naruse, I., D. Kamihashira, Y. Miyauchi, Y. Kato, T. Yamashita, and H. Tominaga. 2005. Fundamental ash deposition characteristics in pulverized coal reaction under high temperature conditions. *Fuel* 84 (4):405–10. doi:10.1016/j.fuel.2004.09.007.

Rushdi, A., A. Sharma, and R. Gupta. 2004. An experimental study of the effect of coal blending on ash deposition. *Fuel* 83 (4–5):495–506. doi:10.1016/j.fuel.2003.08.013.

Sommerfeld, M., and N. Huber. 1999. Experimental analysis and modelling of particle-wall collisions. *Int. J. Multiphase Flow* 25 (6–7):1457–89. doi:10.1016/S0301-9322(99)00047-6.

Thoronton, C., and Z. Ning. 1998. A theoretical model for the stick/bounce behavior of adhesive, elastic-plastic spheres. *Power Technol.* 101:737–58.

Tomeczek, J., and K. Wacławiak. 2009. Two-dimensional modelling of deposits formation on platen superheaters in pulverized coal boilers. *Fuel* 88 (8):1466–71. doi:10.1016/j.fuel.2009.02.023.

Troiano, M., T. Santagata, F. Montagnaro, P. Salatino, and R. Solimene. 2017. Impact experiments of char and ash particles relevant to entrained-flow coal gasifiers. *Fuel* 202:665–74. doi:10.1016/j.fuel.2017.03.056.

Troiano, M., R. Solimene, P. Salatino, and F. Montagnaro. 2016. Multiphase flow patterns in entrained-flow slagging gasifiers: Physical modelling of particle–wall impact at near-ambient conditions. *Fuel Process. Technol.* 141:106–16. doi:10.1016/j.fuproc.2015.06.018.

Vuthaluru, H. B., and D. H. French. 2015. Investigations into the air heater ash deposit formation in large scale pulverised coal fired boiler. *Fuel* 140:27–33. doi:10.1016/j.fuel.2014.09.040.

Walker, K., G. Homsy, and F. Geyling. 1979. Thermophoretic Deposition of Small Particles in Laminar Tube Flow. *J. Colloid Interface Sci.* 69 (1):138–47.

Wall, S., W. John, H. Wang, and S. Goren. 1990. Measurements of kinetic energy loss for particles impacting surfaces. *Aerosol Sci. Technol.* 12 (4):926–46. doi:10.1080/02786829008959404.

Weber, R., Y. Poyraz, M. Mancini, and A. Schwabauer. 2021. Biomass fly-ash deposition: Dependence of deposition rate on probe/particle temperature in 115–1200 °C range. *Fuel* 290:120033. doi:10.1016/j.fuel.2020.120033.

Wei, B., H. Tan, X. Wang, R. Ruan, Z. Hu, and Y. Wang. 2018. Investigation on ash deposition characteristics during Zhundong coal combustion. *J. Inst. Energy* 91 (1):33–42. doi:10.1016/j.joei.2016.11.003.

Xie, J., M. Dong, S. Li, Y. Mei, and Y. Shang. 2018. An experimental study of fly ash particle oblique impact with stainless surfaces. *J. Aerosol Sci.* 123:27–38. doi:10.1016/j.jaerosci.2018.06.001.

Yang, X., D. Ingham, L. Ma, M. Troiano, and M. Pourkashanian. 2019. Prediction of particle sticking efficiency for fly ash deposition at high temperatures. *Proc. Combust. Inst.* 37 (3):2995–3003. doi:10.1016/j.proci.2018.06.038.

Yang, X., D. Ingham, L. Ma, H. Zhou, and M. Pourkashanian. 2017. Understanding the ash deposition formation in Zhundong lignite combustion through dynamic CFD modelling analysis. *Fuel* 194:533–43. doi:10.1016/j.fuel.2017.01.026.

Yu, X., B. Gong, Q. Gao, Y. Zhao, C. Tian, and J. Zhang. 2017. Investigation of fireside corrosion at water-cooled wall from a coal-fired power plant in China. *Appl. Therm. Eng.* 127:1164–71. doi:10.1016/j.applthermaleng.2017.08.053.

Zhou, C., L. Zhang, Y. Deng, and S. Ma. 2016. Research progress on ammonium bisulfate formation and control in the process of selective catalytic reduction. *Environ. Prog. Sustain. Energy* 35 (6):1664–72. doi:10.1002/ep.12409.

Zhou, H., and S. Hu. 2021. Numerical simulation of ash deposition behavior with a novel erosion model using dynamic mesh. *Fuel* 286:119482. doi:10.1016/j.fuel.2020.119482.

Zhou, H., Y. Yang, K. Dong, H. Liu, Y. Shen, and K. Cen. 2014. Influence of the gas particle flow characteristics of a low-NOx swirl burner on the formation of high temperature corrosion. *Fuel* 134:595–602. doi:10.1016/j.fuel.2014.06.027.

Zhou, H., J. Zhang, and K. Zhang. 2018. Investigation of the deposition characteristics of ammonium bisulfate and fly ash blend using an on-line digital image technique: Effect of deposition surface temperature. *Fuel Process. Technol.* 179:359–68. doi:10.1016/j.fuproc.2018.07.030.

Zhou, H., B. Zhou, H. Zhang, and L. Li. 2014. Behavior of fouling deposits formed on a probe with different surface temperatures. *Energy Fuels* 28 (12):7701–11. doi:10.1021/ef502141x.